Tellus (1991), *43A*, 153–167

The diffusive interface at low stability: the importance of non-linearity and turbulent entrainment

By BERT RUDELS, *Institut für Meereskunde, Universität Hamburg, Troplowitzstr. 7, D-2000 Hamburg 54, Germany*

ABSTRACT

The diffusion and convection at low temperature at an interface separating a cold, low salinity upper layer from a warmer, more saline lower layer are examined. The densities of the layers are assumed equal and an approximate, non-linear equation of state is used. The vertical transports are determined from the molecular, diffusive fluxes through the interface. The diffusion creates instabilities at the interface, which convect into the layers. The transition from diffusion to convection is estimated from a Rayleigh number based upon the penetration depth of the density anomaly. The convection occurs as quasi-stationary plumes, maintained by inflow of lighter/denser water, driven by horizontal pressure gradients induced by the density redistribution. The turbulent energy produced in the layers is calculated from the terminal vertical velocity of the buoyant parcels and the horizontal and vertical length scales of the convection. The turbulent energy density is found to depend on layer depth and buoyancy fluxes through the interface cannot be used directly as estimates of the turbulence production. Both turbulent entrainment and the non-linear equation of state could be of less importance for the transport though a diffusive interface in the oceans than what is inferred from corresponding laboratory experiments.

1. Introduction

The molecular properties of sea water, i.e., the non-linearity of its equation of state and the different diffusivities of heat and salt, influence processes of much larger scales and are important in mixing and water mass formation. Many of these phenomena have recently been reviewed by Carmack (1986), who also gives an extensive reference list.

The non-linear effects become especially noticable in the Polar seas. The lowering of the freezing point with pressure, the higher compressibility of colder water and the contraction on mixing or cabbeling, where the mixture of two water masses of similar densities becomes denser than either of the original waters, are all believed important for deep water formation. Another feature of the Polar oceans is the presence of cold surface water overlaying a deeper, warmer water mass. This configuration, with the faster diffusing component (heat) destabilizing, promotes the formation of diffusive interfaces. Deep homogenous layers, vertically separated by thin interfaces, associated with jumps in temperature and salinity, are indeed observed in the Polar seas (Fig. 1). The steps are, especially in the Antarctic, often practically density compensating and the vertical stability between two layers is small. This has made Foster (1972) and Foster and Carmack (1976) suggest that cabbeling might be active in creating and maintaining the observed step structure.

However, McDougall (1981a, b) has shown that for vertically superposed layers, this effect can be treated as a perturbation on a basic double-diffusive convection driven by the unstable distribution of heat. The non-linearity creates a vertical asymmetry of the convection and more buoyancy is released in the lower than in the upper layer. One observable effect of this asymmetry is an upward migration of the interface (McDougall, 1981b). Both processes require that the waters mix down to the molecular level. We shall therefore describe the situation at the interface and estimate the vertical fluxes of heat and salt as well as the migration of the interface assuming only molecular diffusion and a non-linear equation of state.

The discussion of the transfer between the layers (Section 2) is separated into two parts. In Subsec-

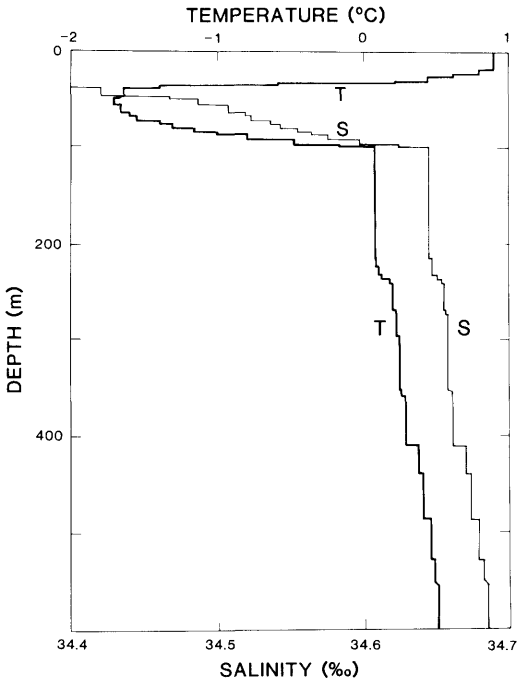

Fig. 1. Temperature and salinity profiles in the Weddell Sea (from Foster and Carmack, 1976).

tion 2.1, the diffusion and the formation of gravitational instabilities are considered, while the dynamic effects of the redistribution of density and the removal of unstable water parcels from the interface are discussed in Subsection 2.2. Some numerical estimates are given in Section 3. The intensity and importance of the turbulence, which may be generated in the layers by the release of buoyancy, are then discussed in Section 4. Finally, in Section 5, the results are compared with laboratory experiments, field observations and some theoretical work. A few of the underlaying assumptions are also discussed.

2. Diffusive transfer across the interface

The horizontal extent of the interface and the depth of the layers are assumed to be infinite. This implies that no external length scale, neither vertical nor horizontal, is imposed. The situation resembles the heated horizontal plate considered by Howard (1967). The diffusion of heat creates an unstable layer close to the plate. The thickness of this layer is determined by the penetration depth $\delta_T = (\pi k_T t)^{1/2}$ of heat (a list of used symbols and some parameter values are given in the appendix). Howard assumed that the evolution of the instability could be described by a Rayleigh number Ra based on the penetration depth. When Ra reaches a critical value ($\sim 10^3$), the unstable parcel convects from the plate and a new cycle begins.

The present case is slightly more complicated with two diffusive components and instabilities forming both above and below the interface. However, Howard's approach will be adopted and the diffusion and the instability are considered in Subsection 2.1. The heated solid plate has no slip boundary conditions and the unstable water will leave the plate as randomly distributed thermals. By contrast, the diffusive interface is a free boundary, which permits horizontal motions. Convection cells may then form, where the unstable water leaves the interface as quasistationary plumes.

This is supported by laboratory observations of evaporative cooling, where the convection occur predominantly as two-dimensional line plumes (Spangenberg and Rowland, 1961). In experiments with the diffusive interface using salt and sugar as diffusing substances (Foldvik and Rudels, 1979), the interface revealed a netted wire structure, where the thin lines were sites of two-dimensional plumes convecting into both layers.

The motions at the interface are generated by the pressure gradients, which arise because of the vertical redistribution of density. A parcel moves along the interface until it becomes unstable and convects into the layers. The spacing of the plumes is thus determined by of horizontal velocity and the time needed for the parcel to become critically unstable. This part of the process is examined in Subsection 2.2.

Subsections 2.1 and 2.2 are extensions and applications of results derived for the linear case (Foldvik and Rudels, 1979).

2.1. Diffusion and instability

An initially sharp horizontal interface separates two infinitely deep layers, the upper slightly colder and fresher than the lower. To maximize the effect of cabbeling the densities of the two layers are taken to be equal. The background temperatures T_1, T_2 and salinities S_1, S_2 in the layers are constant.

The initial conditions are:

$$T_1(z,0)=T_0-\Delta T,\quad S_1(z,0)=S_0-\Delta S,\quad z\geqslant 0,$$
$$T_2(z,0)=T_0+\Delta T,\quad S_2(z,0)=S_0+\Delta S,\quad z<0, \tag{1}$$

and the density ρ is approximated by an equation of state at atmospheric pressure proposed by Mamayev (1975):

$$\rho=A+BT+CT^2+(D-ET)(S-35), \tag{2}$$

where $A=1028.152$, $B=-0.0735$, $C=-0.00469$, $D=0.802$ and $E=-0.002$.

To simplify the writing of the expressions to be derived below, $S'=(S-35)$ is introduced with the primes subsequently dropped and terms containing $ET(S-35)$ are left out. The neglect of these terms is justified for the temperature and salinity ranges ($T\sim 0$, $S\sim 35$) encountered in the Polar seas. However, they may be important in the laboratory experiments and all terms are retained in the computations.

The evolution of the vertical profiles of T and S is described by the solutions to the diffusion equations

$$\frac{\partial T}{\partial t}=k_T\frac{\partial^2 T}{\partial z^2},\qquad \frac{\partial S}{\partial t}=k_S\frac{\partial^2 S}{\partial t^2}, \tag{3}$$

where k_T and k_S are the kinematic diffusion coefficients for heat and salt, taken to be constant. T and S are given by (Crank, 1956)

$$T(z,t)=T_0-\Delta T\,\mathrm{erf}\left(\frac{z}{(4k_T t)^{1/2}}\right),$$
$$S(z,t)=S_0-\Delta S\,\mathrm{erf}\left(\frac{z}{(4k_S t)^{1/2}}\right). \tag{4}$$

Introducing

$$\eta=z(4k_S t)^{-1/2},\quad \tau^{1/2}\eta=z(4k_T t)^{-1/2},\quad \tau=k_S k_T^{-1}, \tag{5}$$

the density anomaly becomes

$$\rho_i'=B\,\Delta T(\pm 1-\mathrm{erf}\,\tau^{1/2}\eta)-C\,\Delta T^2(1-\mathrm{erf}^2\,\tau^{1/2}\eta)$$
$$+2CT_0\,\Delta T(\pm 1-\mathrm{erf}\,\tau^{1/2}\eta)+D\,\Delta S(\pm 1-\mathrm{erf}\,\eta). \tag{6}$$

$i=1,2$ indicates the upper and lower layers and for $i=1$, $\eta\geqslant 0$ and the upper sign is used and for $i=2$, $\eta<0$ and the lower sign holds. The profiles of T and S, of the density contributions due to T and S and the profile of ρ are sketched in Fig. 2 a–c for $t=0$, $t=t_1$ and $t=t_2$.

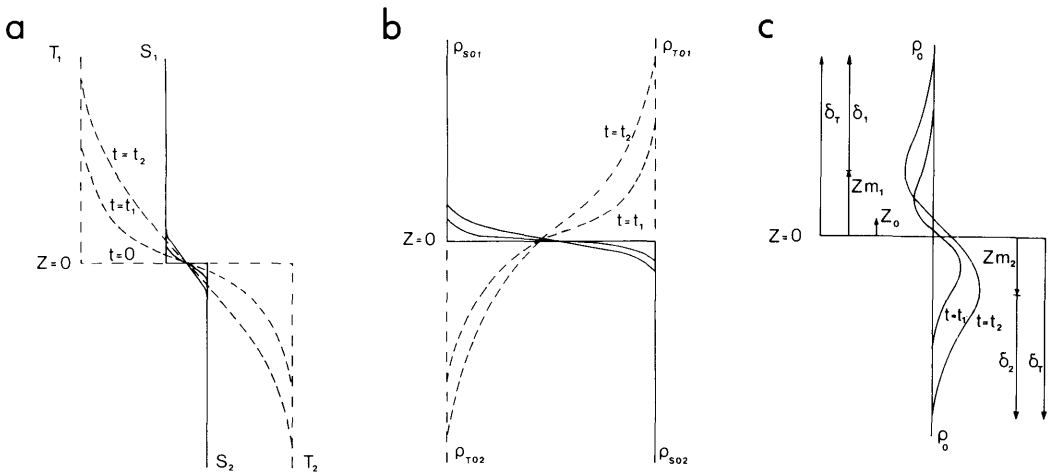

Fig. 2. Qualitative sketch of the evolution of the vertical profiles of (a) temperature T and salinity S; (b) density due to heat ρ_T and due to salt ρ_S; (c) the density profile ρ, with time. Broken lines indicate profiles due to T, solid lines due to S. The penetration depth of heat δ_T, the levels of maximum density anomaly z_{m_1}, z_{m_2} and the level of no density anomaly z_0 are indicated. δ_1, δ_2 are the penetration depths used in the Rayleigh number. The profiles are sketched to show the effects of the non-linearity, the larger density changes due to temperature variations at higher temperatures and the vertical migration of the level of zero density anomaly.

Following Howard we write:

$$\mathrm{Ra} = \frac{g\,\Delta\rho_i \delta_i^3}{\rho_0 \nu k_T}, \tag{7}$$

where ν is the coefficient of viscosity, $\delta_i = \delta_T - z_{m_i}$ gives the distance of the penetration of heat beyond the levels of maximum density anomaly z_{m_1} and z_{m_2}.

$$\Delta\rho_i = \delta_i^{-1} \int_{z_{m_i}}^{\infty} \rho^1 \, dz$$

is the average density anomaly for the parcel above (below) z_{m_i} (z_{m_2}). Using the identity $\mathrm{erf}\,\eta = (1 - \mathrm{erfc}\,\eta)$ and the symmetry properties of the error function, eq. (6) can be written as

$$\rho_i' = \pm (B + 2C(T_0 \mp \Delta T))\,\Delta T\,\mathrm{erfc}\,\tau^{1/2}\eta \pm D\,\Delta S\,\mathrm{erfc}\,\eta + C\,\Delta T^2\,\mathrm{erfc}^2\,\tau^{1/2}\eta, \tag{8}$$

where now $\eta \geqslant 0$ for both $i = 1$ and $i = 2$. $\Delta\rho_i$ then becomes

$$\Delta\rho_i = \frac{(4k_S t)^{1/2} F_i}{\delta_i} \tag{9}$$

with

$$F_i = \pm (B + 2C(T_0 \mp \Delta T))\,\Delta T \int_{\eta_{m_i}}^{\infty} \mathrm{erfc}\,\tau^{1/2}\eta \, d\eta \pm D\,\Delta S \int_{\eta_{m_i}}^{\infty} \mathrm{erfc}\,\eta \, d\eta + C\,\Delta T^2 \int_{\eta_{m_i}}^{\infty} \mathrm{erfc}^2\,\tau^{1/2}\eta \, d\eta, \tag{10}$$

and the Rayleigh number can be written as

$$\mathrm{Ra} = \frac{2gF_i k_S^{1/2} \pi (1 - 2\eta_{m_i}(\tau\pi^{-1})^{1/2})^2\, t^{3/2}}{\rho_0 \nu}. \tag{11}$$

We use the classical value $27\pi^4/4$ as critical Rayleigh number (Chandrasekhar 1961) and solving equation 11 for t_{i*} gives

$$t_{i*} = \left[\frac{27\pi^3 \rho_0 \nu}{8gF_i k_S^{1/2} (1 - 2\eta_{m_i}(\tau\pi^{-1})^{1/2})^2} \right]^{2/3}, \tag{12}$$

where the subscript $_*$ indicates critical values.

m_i can be found from $d\rho_i'/dz = 0$, and the use of eq. 6 leads to

$$e^{\eta_{m_i}^2(1-\tau)} + \frac{D\,\Delta S}{\tau^{1/2}\,\Delta T(B + 2C(T_0 - \Delta T\,\mathrm{erf}\,\tau^{1/2}\eta))} = 0. \tag{13}$$

Eq. 13 can be solved numerically for η_{mi} and t_{i*} is then determined from eq. (12).

Since the coefficient of viscosity is larger than the diffusion coefficients, the motions in the two layers will be coupled across the interface (see Section 2.2). When Ra_* is reached on one side the convection will also be triggered on the other side and the smallest value t_{i*} is used. With t_* known δ_{i*} and z_{mi*} can be determined from eq. (5) and the definition of δ_i. We assume that not only the parts above and below z_{mi*} but all unstable fluid is removed by the convection. The level z_{0*} are found by putting $\rho' = 0$ in eq. 8 and use eq. (5) and t_*. The removal of unstable water reestablishes the initial conditions. However, the position of the interface will migrate upwards following z_0. This is in accordance with the work by McDougall (1981a, b).

2.2. *Convection and removal of unstable fluid*

The free interface allows horizontal motions and the convection may occur as quasi-stationary plumes as indicated by the observations of Spangenberg and Rowland (1961) and Foldvik and Rudels (1979). The plumes are assumed two-dimensional and are maintained by a horizontal inflow of marginally unstable fluid. The flow is stationary and occurs in a plane perpendicular to the plume. The plumes are of finite length and the description breaks down at the points where several plumes meet. However, since the length of the plumes are of the same order as the plume spacing these points will occupy only a small part of the interface and can be ignored.

When two parcels come in contact across the interface, diffusion of heat and salt begins and instabilities form and grow as the parcels are advected towards the plumes. The time dependent solution obtained in the preceeding section thus applies for the individual, moving parcels. The motion towards the plumes is driven by the horizontal pressure gradient and the evolving density field enforces any horizontal displacement of the parcels. The horizontal motion is coupled

across the interface by the pressure gradient and by viscosity. The density distribution and the velocity filed between two plumes are shown in Fig. 3.

The spacing, $2L_*$, between the plumes is determined by t_* and the horizontal velocity U at the interface. Since $W/U \sim \delta_{i*}/L_* \ll 1$ at the interface outside the plumes, the vertical velocity can be ignored in the diffusive regime. The horizontal momentum equation then takes the form:

$$U\frac{\partial U}{\partial x} = -\rho^{-1}\frac{\partial p'}{\partial x} + \nu\frac{\partial^2 U}{\partial z^2}, \tag{14}$$

where the term $\nu(\partial^2 U/\partial x^2)$ has been neglected. ρ is the average density and $p' = \int_z^\infty g\rho'\,dz'$ is the perturbation pressure created by the diffusion.

By integrating vertically across the interface and letting $z \to \infty$ the limits of integration are taken outside the viscous boundary layer. The friction terms then vanish ($U = 0$) and the sequence of integration and differentiation may be changed. Eq. (14) then becomes

$$\frac{\partial}{\partial x}\left[2^{-1}\int_{-\infty}^{\infty} U^2\,dz + \rho^{-1}\int_{-\infty}^{\infty} p'\,dz\right] = 0. \tag{15}$$

The expression inside the brackets is independent of x and shows that the total energy is conserved for a parcel following the motion. Since U and p' are 0 at $x = 0$, the mid-point between the plumes, the constant is zero.

Separating the integration over the two half-planes and introducing the expression for p' and the results from eq. (2.1) lead to

$$\begin{aligned} 0 = {} & 2^{-1}\int_0^\infty U^2\,dz + 2^{-1}\int_{-\infty}^0 U^2\,dz \\ & + \left[\frac{4k_S g}{\rho}\right]\Bigg[(B + 2C(T_0 - \Delta T)) \\ & \times\frac{\Delta T}{4\tau} + \frac{D\,\Delta S}{4} + C\,\Delta T^2 \\ & \times\int_0^\infty d\eta\int_0^\eta \operatorname{erfc}^2 \tau^{1/2}\eta'\,d\eta'\Bigg] t \\ & + \left[\frac{4k_S g}{\rho}\right]\Bigg[-(B + 2C(T_0 + \Delta T)) \\ & \times\frac{\Delta T}{4\tau} - \frac{D\,\Delta S}{4} + C\,\Delta T^2 \\ & \times\int_0^\infty d\eta\int_0^\eta \operatorname{erfc}^2 \tau^{1/2}\eta'\,d\eta'\Bigg] t. \end{aligned} \tag{16}$$

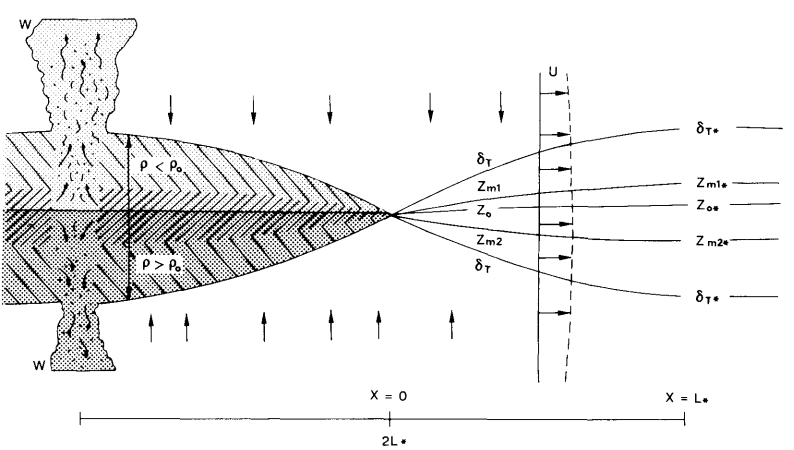

Fig. 3. The density field (to the left) and the velocity field (to the right) for the diffusive region between two convecting plumes. U is the horizontal velocity at the interface and $2L_*$ the plume spacing. Light shading indicates $\rho < \rho_0$, dark shading $\rho > \rho_0$. Regions of unstable density gradients are shown with sparsely spaced lines slanted to the left while the region of stable gradient is given with densely spaced lines slanted to the right. Starred quantities indicate critical values. Other symbols as in Fig. 2.

We introduce

$$M_1 = 2^{-1}\rho \int_0^{\infty} U^2 \, dt,$$
$$M_2 = 2^{-1}\rho \int_{-\infty}^{0} U^2 \, dz, \tag{17}$$

where M_1 and M_2 are the kinetic energies, which have been induced in the two layers by the density redistribution. The linear case is symmetric around $z = 0$, but eq. (16) shows that the 4th term is larger than the 3rd, which would imply that more kinetic energy is generated in the lower than in the upper layer, and a velocity jump should occur at $z = 0$. However, the total mass is conserved and no motion is present below the region affected by the diffusion. This means, in reality, that the free upper surface is lowered to add a barotropic pressure gradient. Since the depth is assumed infinite this effect is not taken into account. The density changes below $z = 0$ must cancel all pressure changes occurring in the upper half plane and by equating the 2nd and the 4th terms in eq. (16) an approximation holding for the kinetic energy generated in each of the layers should be obtained.

The velocity of the parcels is not constant. Moreover, the velocity spreads into the layers by viscosity. We shall assume that the gross features of the velocity field can be described by the diffusion equation

$$\frac{\partial U}{\partial t} = \nu \frac{\partial^2 U}{\partial z^2}, \tag{18}$$

applied at a coordinate system following the motion. This means that the effects of advection on the velocity field is ignored.

Since U and U^2 will have the same diffusivity ν, M can be regarded as the result of a diffusion of kinetic energy from a boundary into a half plane. There should then be a corresponding kinetic energy "concentration" $m_0 = m(0, t)$ at the interface. Standard texts on diffusion problems, e.g., Crank (1956), p. 31, give the relation

$$M = 2^{-1} m_0 (\pi \nu t)^{1/2} \tag{19}$$

for the amount diffused into a half plane, when m_0 is time-dependent. In the present case, the time dependence of M is known ($= t$) which requires m_0 to be

$$m_0 = \left[\frac{8 k_S g G}{\nu^{1/2} \pi^{1/2}}\right] t^{1/2}, \tag{20}$$

where G is the expression inside brackets in the fourth term of eq. (16), and the velocity at the interface becomes:

$$U_0 = \left[\frac{16 k_S g G}{\rho \nu^{1/2} \pi^{1/2}}\right]^{1/2} t^{1/4}. \tag{21}$$

Because $\nu > k_T \gg k_S$, the velocity in the diffusive boundary layer can be considered independent of z and equal to U_0.

The distance L_* a parcel moves before it enters the plume is found by integrating (21) from $t = 0$ to $t = t_*$

$$L_* = \tfrac{4}{5} c t_*^{5/4}, \tag{22}$$

and the spacing between the plumes becomes $2L_*$. The finite length of the line plumes leads to a polygonic convection pattern resembling the cells occurring in ordinary Benard convection (Spangenberg and Rowland, 1961; Foldvik and Rudels, 1979). However, the horizontal extent of the cells is orders of magnitudes larger than the corresponding Benard cells obtained for a depth comparable to δ_T.

The amount N of buoyancy, heat or salt, which enters the plumes from one side is

$$N_* = U_* \int_{z_{0_*}}^{\infty} f \, dz, \quad f = \text{concentration}, \tag{23}$$

and the flux per unit area between the layers becomes

$$\phi_* = N_* L_*^{-1} = \frac{5}{4} t_*^{-1} \int_{z_{0_*}}^{\infty} f \, dz. \tag{24}$$

The factor $\frac{5}{4}$, recognized in Foldvik and Rudels (1979), indicates that plumes are more efficient than thermals in transferring heat and salt across the interface.

3. Numerical results

The non-linearity of the equation of state is largest at low temperature, and since the most

interesting ranges and steps are those encountered in the Weddell Sea (Fig. 1) temperature steps of 0.1°C and 1°C are chosen. The larger value is seldom found outside frontal areas and may be regarded as an upper limit. To compare the results with those of McDougall (1981b) the concentrations in one of his experiments are also examined.

The initial values, T_1, T_2, S_1 and S_2 are given in Table 1. S_2 has been computed from equation 2 with $\rho_{01} = \rho_{02}$. Table 1 also gives t_*, δ_{i*} and z_{0*}. Finally the migration velocity for the interface, $w_* = 1.25 z_{0*} t_*^{-1}$ is given. The factor 1.25 arises from the assumption of plume convection. To show the magnitude of the non-linearity the values in the tables are given with several digits. This does not represent the accuracy of the model predictions.

The thickness of the unstable layer is about 0.001 m in the laboratory and 0.01 m in the ocean. The effect of the non-linearity, as estimated by the ratio $z_{0*}\delta_{i*}^{-1}$, is much larger in the laboratory (about a factor of 100). This is partly due to the stronger non-linearity of the temperature and salinity range covered in the laboratory, partly due to larger gradients. The weaker gradients in the oceans lead to time-scales 100 times as long as in the laboratory. These effects combine to give a small migration velocity in the ocean.

The fluxes of heat and salt between the layers are given in Table 2. The asymmetry in the transports is due to the upward migration of the interface. The incorporation of a volume of colder, fresher water into the lower layer shows up as a loss of heat and salt in that layer. The ratio of the density

Table 1. *The initial temperatures, salinities and densities for the three considered cases and the properties derived for the instability at the interface (for symbols see text)*

	a	b	c
T_1 (°C)	−0.05	−0.50	4.00
T_2 (°C)	+0.05	+0.50	30.00
S_1	34.65	34.65	0.0
S_2	34.659	34.741	5.71
ρ_0 (kg m^{-3})	1027.87	1027.91	1000.00
t_{1*} (s)	1350	300	34
t_{2*} (s)	1340	280	13.4
δ_{1*} (m)	$17.0 \cdot 10^{-3}$	$7.8 \cdot 10^{-3}$	$1.69 \cdot 10^{-3}$
δ_{2*} (m)	$17.0 \cdot 10^{-3}$	$7.8 \cdot 10^{-3}$	$1.71 \cdot 10^{-3}$
z_{0*} (m)	$0.008 \cdot 10^{-3}$	$0.036 \cdot 10^{-3}$	$0.096 \cdot 10^{-3}$
w_* (m s^{-1})	$0.007 \cdot 10^{-6}$	$0.156 \cdot 10^{-6}$	$8.955 \cdot 10^{-6}$

Table 2. *Fluxes of heat, salt and buoyancy between the layers for the three cases*

	a	b	c
Heat flux (W m^{-2})			
into $z \geqslant z_{0*}$	2.55	55.2	$6.15 \cdot 10^{3}$
out of $z \leqslant z_{0*}$	2.55	56.1	$7.11 \cdot 10^{3}$
salt flux (kg m^{-2} s^{-1})			
into $z \geqslant z_{0*}$	$5.5 \cdot 10^{-9}$	$0.114 \cdot 10^{-6}$	$15.1 \cdot 10^{-6}$
out of $z \leqslant z_{0*}$	$5.6 \cdot 10^{-9}$	$0.128 \cdot 10^{-6}$	$66.0 \cdot 10^{-6}$
Buoyancy flux (W m^{-3})			
into $z \geqslant z_{0*}$	$0.388 \cdot 10^{-6}$	$8.10 \cdot 10^{-6}$	$0.97 \cdot 10^{-3}$
into $z \leqslant z_{0*}$	$-0.392 \cdot 10^{-6}$	$-9.00 \cdot 10^{-6}$	$-3.81 \cdot 10^{-3}$

Table 3. *The horizontal velocity at the interface U_* and the half-spacing L_* between the plumes for the three cases*

	a	b	c
U_* (m s^{-1})	$0.5 \cdot 10^{-3}$	$1.1 \cdot 10^{-3}$	$4.8 \cdot 10^{-3}$
L_* (m)	0.53	0.24	0.05

flux due to salt to that due to heat is close to $(k_S k_T^{-1})^{1/2}$ as it should when only molecular transports are considered (Turner, 1973).

While heat and salt are transported between the layers, buoyancy is released in both layers. The asymmetry of the release depends strongly on the concentration steps. Table 2 gives the buoyancy carried by the particles as they leave the interface. To estimate the final asymmetry of the buoyancy release the depths of the layers must be known.

The horizontal velocity at the interface is about 0.001 ms^{-1} in the ocean and the spacing of the plumes 0.5–1m (Table 3). Since the width of the plumes should be of the same order as the thickness of the unstable layer the plumes occupy only 3–4% of the interface. The vertical return flow outside the plumes is therefore weak. In the laboratory the horizontal dimensions are smaller but the velocities higher. Because of the larger velocities the return flow is more intense in spite of a similar ratio $\delta_{i*} L_*^{-1}$ between areas of upward and downward motions.

4. The turbulent activity in the layers

The effects of turbulence on the transports through the interface have up to now been ignored. However, the convection itself generates turbulence in the layers, which may increase the fluxes above that of molecular diffusion. The neglect of turbulence in the preceding sections should therefore be justified. To elaborate this point, we follow the discussion given by McDougall (1981b, Section 52).

Externally generated turbulence creates an entrainment velocity e, which, in a two-layer system, transports mass against gravity across the interface. The ratio of e to the representative r.m.s. velocity u_* of the turbulence is found from experiments to be (Turner, 1973).

$$\frac{e}{u_*} = k_1 \left(\frac{u_*^2}{g \Delta_{\rho H}} \right)^n, \tag{25}$$

where H is the layer depth. The values of the constants are not accurately known. The exponent n, which is of the greater interest, is 1 for systems stratified by heat and 1.2–1.5 for salt stratified systems (Turner, 1973; McDougall, 1981b). For $n = 1$ eq. (25) becomes

$$k_1 = \frac{g \Delta \rho e H}{u_*^3}, \tag{26}$$

which shows that in this case the gain in potential energy is proportional to the input rate of external energy to the turbulence (Turner, 1973).

The turbulent energy ε produced by the buoyancy flux Q can be written as

$$\varepsilon = u_*^3 H^{-1} = k_2 Q, \tag{27}$$

and if eqs. (26) and (27) are combined, the entrainment velocity becomes

$$e = \frac{k \rho Q}{g \Delta \rho}, \qquad k = k_1 k_2, \tag{28}$$

which makes e independent of the layer depth. This results because, when using eq. (26), it is assumed that the mass is transferred from the center of one layer to the center of the other. The deeper the layer, the more potential energy is released and the turbulent energy density remains constant.

However, the released potential energy must first be transformed into kinetic energy by the rising and sinking of buoyant parcels, and to generate the prescribed turbulent energy these must accelerate over the entire depth H. The parcels are small and their motions dominated by viscosity and they will rise with a velocity determined by a balance between buoyancy and viscosity. Any further distance, which they travel after they have attained this "terminal" velocity, will not make more energy available for the turbulence, apart from the weakly energetic motion added to the environment directly by the viscosity. This implies that there exists an optimal depth for generating turbulent energy by buoyancy flux and this depth should be used in eqs. (26) and (27).

The arguments leading to eq. (28) then hold only for the depth over which the parcels accelerate. If the layer is thinner, the parcels will not attain the terminal velocity before they reach the other boundary and stratification, not turbulence, is created in the layer. When the layer is deeper, the turbulence is distributed over a larger volume and the energy density will be smaller.

The velocity W_0 of the parcels may be estimated from Stokes' resistance law (Batchelor, 1967; Subsection 4.9). The density anomaly of the parcels is $\Delta\rho_{i*}$, but to take into account the doubling of the volume, which results from the merging of two unstable parcels at the region of convection, we write the diameter of the convecting parcel as: $\delta_{pi} = 3\sqrt{2}\,(\delta_{T*} \mp z_{0*})$. The vertical velocity then becomes:

$$W_{0i} = \frac{g\,\Delta\rho_* \delta_{pi}^2}{15\rho\nu}, \tag{29}$$

which is comparable to the horizontal velocity U_{0*} (Tables 3, 4). W_0 should be reached when the effects of viscosity have penetrated to the center of the parcel. The time necessary for this is of the same order as the time needed for the parcel to become unstable and the acceleration should occur over a distance comparable to that of the horizontal acceleration L_*, determined in Subsection 2.2. However, if no physical boundary or no density stratification is present, the buoyant parcels will continue to rise/sink and the turbulent energy is distributed over a layer deeper than L_*.

The maximum vertical distance H_0, which a buoyant parcel may rise, depends upon how fast the density anomaly diffuses out of the parcel. Using an expression given by Turner (1973) we have

$$\Delta\rho_i = \Delta\rho_{i*} \exp[-k_\tau t(\pi\delta_{pi}^2)^{-1}]. \tag{30}$$

Table 4. *The terminal velocity W_0 and the maximum vertical distance H_0 traversed by the parcels for the three cases*

	a	b	c
W_{01} (m s^{-1})	$0.60 \cdot 10^{-3}$	$1.20 \cdot 10^{-3}$	$1.43 \cdot 10^{-3}$
W_{02} (m s^{-1})	$0.61 \cdot 10^{-3}$	$1.34 \cdot 10^{-3}$	$6.19 \cdot 10^{-3}$
H_{01} (m)	12.6	5.2	0.27
H_{02} (m)	12.8	5.9	1.42

Integrating from $t = 0$ to infinity leads to

$$H = \frac{\pi g\,\Delta\rho_{i*}\delta_{pi}^4}{15\rho\nu k_\tau}. \tag{31}$$

H_0 depends upon the temperature gradient and smaller steps leads to larger depths.

The turbulent energy density is calculated using eq. (27), W_0 and taking either L_* or H_0 as the scale of the energy containing eddies. ε based on both scales are given in Table 5. When L_* is used, the energy production agrees with the buoyancy release found in Section 2 (Table 2) for small steps, but for the laboratory case the energy production becomes one order of magnitude smaller. This might be due to the small ($\delta_{pi} \sim 10^{-3}$ m) size of the convecting parcels, which leads to large direct viscous dissipation and thus decreases the energy otherwise available for turbulence production. A turbulent energy density based on H_0, would give a measure of the minimum turbulent activity in a system dominated by diffusive fluxes. The result indicates that L_* might be a useful approximation of the eddy size, and turbulent energy densities could be estimated by the buoyancy release multiplied by the ratio of L_* to the observed layer depth. A stronger turbulence is present in the laboratory experiment, where the layer depths are of the same order as L_*. Because of the nonlinearity the turbulence is 20 times as intense in the lower as in the upper layer. By comparison the turbulent activity is low in the oceans and almost equal in the two layers (Table 5).

We try to estimate the turbulent entrainment velocity across the interface by writing eq. (26) as

$$e = u_* \frac{\rho u_*^2}{g\,\Delta\rho H} = u_* \mathrm{Ri}^{-1}, \tag{32}$$

where Ri is the Richardson number (see also Turner, 1973, chapter 9). Ri gives the relative importance of stratification and velocity shear. Since the layers have the same density one should expect Ri to be zero, leading to turbulence and complete overturning.

However, the evolution of the density profile caused by the diffusion creates a stable density gradient between z_{m_1} and z_{m_2} (Fig. 2c) and the density jump $\Delta\rho$ can be estimated from eq. (6) as $2^{-1}\,(\rho'(z_{m_2}) - \rho'(z_{m_1}))$. By contrast, no shear is present, since the motions in the two layers are

Tellus A 43 2-6

Table 5. *Rate of turbulent energy production in the two layers for the three cases*

	a	b	c
$\varepsilon_i = W_{0i}^3 L_*^{-1}$			
ε_1 (W m^{-3})	$0.41 \cdot 10^{-6}$	$7.2 \cdot 10^{-6}$	$0.056 \cdot 10^{-3}$
ε_2 (W m^{-3})	$0.43 \cdot 10^{-6}$	$10.0 \cdot 10^{-6}$	$0.456 \cdot 10^{-3}$
$\varepsilon_i = W_{0i}^3 H_{0i}^{-1}$			
ε_1 (W m^{-3})	$0.017 \cdot 10^{-6}$	$0.331 \cdot 10^{-6}$	$0.011 \cdot 10^{-3}$
ε_2 (W m^{-3})	$0.018 \cdot 10^{-6}$	$0.399 \cdot 10^{-6}$	$0.167 \cdot 10^{-3}$

coupled and parallel at the interface. The velocity and length scales in eq. (32) must therefore be related to the motions in the layers as in the stirring grid experiments (Turner, 1973).

The grid experiments show that the entrainment decreases with the distance from the oscillating grid. The velocities important for the entrainment would then be those close to the interface, connected with the weak return flow, which is only $\frac{1}{25}$ of the plume velocity W_0 (Section 3). The use of $W_0/25$, H_0 and the $\Delta\rho$ obtained from eq. (6) gives $\mathrm{Ri} \sim 0.6 \cdot 10^6$ for all cases. This is stable and the entrainment velocity becomes (for case (a)) less than $\frac{1}{100}$ of the migration velocity w_* given in Table 1. The ratio e/w_* becomes smaller as the gradients increase since w_* depends more strongly on the concentrations than W_0 (Tables 1, 4).

The formation of a stable interfacial density gradient may effectively prevent convectively generated turbulence from entraining water across the interface. However, the density difference between the layers is still zero. Buoyant parcels generated by cooling and heating at the upper and lower boundaries could easily pass through the layers, penetrate through the interface and transfer mass between the layers.

5. Discussion

5.1. *Comparison with other work*

The present work states the case for the importance and dominance of molecular processes, also at low stability ratios $R_\rho = \rho_S \rho_T^{-1}$, for the transfer of heat and salt through a diffusive interface. The model applies for $R_\rho = 1$. When $R_\rho > 1$ water of intermediate density is produced and accumulates at the interface. However, at least for $R_\rho \leqslant 1.5$ this accumulation is small enough to be ignored. It may be considered as an extension of the work by Linden and Shirtcliffe (1978) to a regime, where no stable, diffusive layer of intermediate density can be maintained at the interface. The approach especially differs from that in the model of Fernando (1989), where turbulence dynamics, once the convection is established, dominates the buoyancy transfer.

As in the Linden and Shirtcliffe model the buoyancy flux due to heat F_T follows, for the linear case, a $(g\rho_T)^{4/3}$ law, given by

$$F_T = \frac{\left(\begin{array}{c} 1.25[g\rho_T]^{4/3}\,[\mathrm{ierfc}\,\tau^{1/2}\eta - R_\rho \tau^{1/2}\,\mathrm{ierfc}\,\eta] \\ \times \pi^{1/3} k_T^{2/3} (1 - 2(\tau\pi^{-1})^{1/2})^{2/3} \end{array}\right)}{\left[\frac{27\pi^4}{4} v\right]^{1/3}} \tag{33}$$

where ierfc is the first integral of the error function. For $R_\rho = 1$ this becomes

$$F_T = \frac{5}{3}\left(\frac{k_T^2}{\pi^5 v}\right)^{1/3} (g\rho_T)^{4/3} (1 - \tau^{1/2})^{4/3}. \tag{34}$$

To arrive at this simpler expression, the penetration depth has been computed from z_0. The heat flux is about $\frac{1}{4}$ of the value estimated by Huppert 1971 for $R_\rho = 1$ and as in the work by Linden and Shirtcliffe the ratio of the buoyancy fluxes is given by $\tau^{1/2}$.

The $\frac{4}{3}$ law has recently been examined by Kelley (1990) who argues that this law only holds for a free-slip interface while a no-slip boundary condition would give a different exponent. While the no-slip condition may be appropriate for large R_ρ, our discussion in Subsection 2.2 has shown that this should not be so for R_ρ close to 1 and the $\frac{4}{3}$ law should apply for the present case.

In Turner's two layer laboratory experiments, where colder, fresher overlaid warmer, saltier water (Turner, 1965), the ratio of the density flux

due to salt, to that due to heat was $(k_S k_T^{-1})^{1/2}$ for R_ρ larger than 2. When R_ρ decreased from 2 to 1, the flux ratio increased towards 1. The increase in flux ratio indicates that turbulence was transporting water, heat and salt between the layers. However, in the experiments the lower layer was heated from below and external turbulence introduced into the system. In salt-sugar experiments the flux ratio remained at $(k_S k_T^{-1})^{1/2}$ for as low R_ρ as has been reached (Shirtcliffe, 1973). In McDougall's experiments no heating was present once the runs were started and he reports a flux ratio close to $\tau^{1/2}$ at least for R_ρ down to 1.5 (McDougall, 1981b).

McDougall observed a migration of the interface and the vertical displacement corresponding to our case (c) can be estimated from Fig. 3 in McDougall's work to be 0.015 m in 15 minutes. During this time the migration should, according to Table 1 be 0.008 m. About 50% can be accounted for by molecular diffusion and non-linearity. If the turbulence is, as in case (c), asymmetrically distributed about the interface water will be drawn from the less into the more active layer, and result in a migration of the interface. However, this contribution should, according to Section 4, be negligible also in McDougall's experiments, which then does not appear to be the case.

The depth of the layers was 0.3 m, substantially smaller than the $H_0 \sim 1.4$ m obtained for the more energetic layer in case (c). This affects u_* since the deflection of the plumes at the upper and lower boundaries would intensify the return flow. Increasing u_* and decreasing H each by a factor of 5 in eq. (32), would give an additional, turbulent entrainment velocity of about 10% of w_*. An other factor, which may be responsible for the discrepancies, is the mechanically generated turbulence present just before the start of the experiment. A different choice of δ in the Rayleigh number could also lead to a larger migration velocity (see below). In any case expected displacement of the interfaces in the ocean is small and amounts to 1 m per year.

There are few measurements of double-diffusive fluxes in the ocean. The study of heat fluxes and turbulent dissipation in a diffusively convecting region made by Schmitt et al. (1986) indicates that fluxes determined from laboratory experiments overestimate both the heat transport and the buoyancy release by a factor of 5 to 10. However, Schmitt et al. compare buoyancy release with the observed dissipation of turbulence without considering the depth of the layers. The density ratio was about 1.3 and it should be possible to use the present approach. If temperature steps of 0.4°C and layer depths of 2 m, are considered, the heat transport using eq. (33) becomes 17.5 Wm^{-3}, perhaps 50% larger than the value estimated by Schmitt et al. (1986). The turbulence production obtained by multiplying the buoyancy flux with LH^{-1}, where H is half the layer depth, is $0.6 \cdot 10^{-6}$ Wm^{-3}, less than 10% of the observed dissipation. This in spite of the use of the flux ratio $(\rho_S \rho_T^{-1})^{1/2}$, which gives a higher ratio of buoyancy release to heat flux than the laboratory results. If the buoyancy release is used to estimate the turbulence production it is still less than half the observed dissipation.

However, it is not clear from the table presented by Schmitt et al. what observed values are used. With the steps considered here the heat flux, obtained from Huppert's expression would have been 40 Wm^{-3} instead of the given 115 Wm^{-3}.

The layer structure observed in connection with diffusive interfaces has recently been examined by Federov (1988) and Kelley (1984, 1988). Since these authors consider the entire range of R_ρ, this is not the place to examine their work in detail. However, an estimate of layer depth was derived in Section 4 and it might be illuminating to look at the low stability end point of their studies.

Kelley (1984, 1988) scales the observed layer depth H as

$$G = \frac{H}{\left(\dfrac{k_T}{((g/\rho)\, \mathrm{d}\rho/\mathrm{d}z)^{1/2}} \right)^{1/2}}, \tag{35}$$

and by examining several thermohaline staircases he obtains the relation shown in Fig. 4 (adapted from Kelley, 1988). The layers reported by Foster and Carmack (1976), (Fig. 1) were not included in the original figure. The R_ρ for the deeper layers is about 1.03 (Foster and Carmack, 1976) and $(g/\rho)\, \mathrm{d}\rho/\mathrm{d}z$ can be estimated to $2.09 \cdot 10^{-8}$ s^{-2}. The layer depth is about 40 m (Fig. 1). Entering these values into equation (35) gives $G \sim 1500$, which is out of the range suggested by the other points in Fig. 4.

The reason for this discrepancy is most likely the low stability ratio. If linear gradients of T, S and ρ

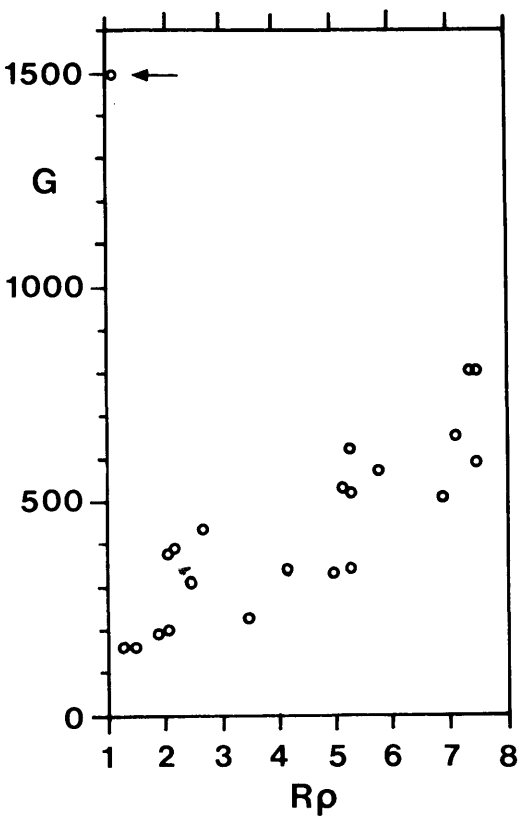

Fig. 4. G = layer thickness divided by $(k_T/(g/\rho)\ d\rho/dz)^{1/2})^{1/2}$ versus density ratio R_ρ. The position of the layers reported by Foster and Carmack (1976), which were not included in the original figure, are indicated (adapted from Kelley, 1988).

are disturbed to form a step (Fig. 5), the density anomaly of the parcels forming above and below the step will be given by

$$\delta_\rho = \frac{\Delta\rho_T}{\pi}(1 - R_\rho \tau^{1/2}) \sim 0.3\Delta\rho_T, \tag{36}$$

for $R_\rho = 1$ and using a linear equation of state. However, since

$$\rho_T = H\frac{d\rho_T}{dz}, \qquad \Delta\rho = H(1 - R_\rho)\frac{d\rho}{dz}$$

the density steps created by the disturbance can never, for $R_\rho \leqslant 1.2$, be large enough to confine a buoyant parcel to the initial layer and it will rise until the heat has diffused out as was suggested in section four. If only two layers are created this would hold up to $R_\rho \sim 1.5$ (Fig. 5).

Since H_0 goes as $(\rho_T)^{-1/3}$, the expected rise for $\Delta T \sim 0.05°C$ can be estimated from Table 4 to be ~ 15 m which is about half the value observed in Fig. 1. For larger R_ρ the initial density jumps will limit the vertical extent of the convection. This is perhaps confirmed by the much smaller thicknesses in the upper part in Fig. 1 and by the thinner layers in Schmitt et al., 1986. This difference between small and intermediate and large stability ratios could explain the anomalous position of the low stability layers in Fig. 4.

One reason for examining the layer height is to obtain an effective eddy diffusivity k_E for heat and salt to be used with the overall property gradients. The fluxes across each layer would then be given

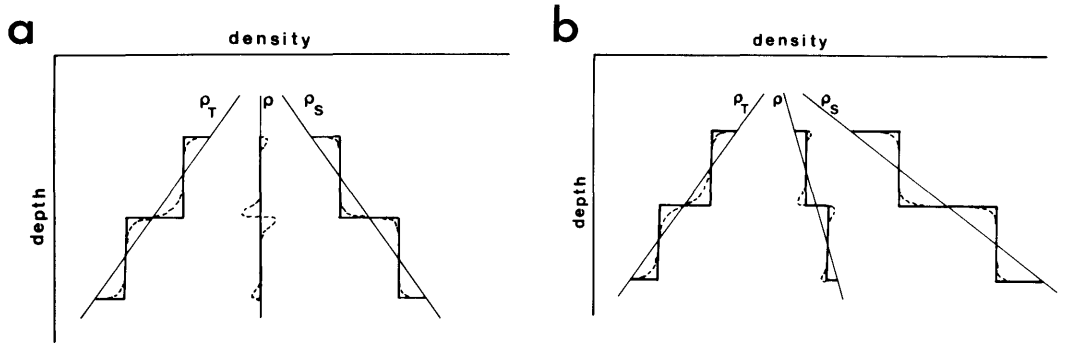

Fig. 5. The evolution of vertical profiles of ρ_T, ρ_S and ρ after a disturbance creating two homogeneous layers. Thin lines = initial profiles. Heavy lines = the profiles immediately after the disturbance. Broken lines = the evolution of the profiles due to diffusion. (a) $R_\rho = 1$; (b) $R_\rho = 1.5$.

by the flux law (eq. (33)) together with the temperature step.

$$\Delta\rho_T = H_0 \frac{d\rho_T}{dz}. \tag{37}$$

For $R = 1$, we have:

$$k_{TE} \frac{d\rho_T}{dz} = \frac{5}{3}\left(\frac{k_T^2 g}{\pi^5 \nu}\right)^{1/3} \times (\Delta\rho_T)^{4/3} (1 - \tau^{1/2})^{4/3}, \tag{38}$$

and by using eq. (37) we obtain

$$k_{TE} = \frac{5}{3} H_0 (\Delta\rho_T)^{1/3} \times \left(\frac{k_T^2 g}{\pi^5 \nu}\right)^{1/3} (1 - \tau^{1/2})^{4/3}. \tag{39}$$

After introducing the expression for H_0 (eq. (31)) and using linear expressions for $\Delta\rho_i$ and δ_{ρ_i}, this becomes:

$$k_{TE} = \frac{g\pi^5}{2^{4/3}} (1 - \tau^{1/2}) k_T = 980 k_T, \tag{40}$$

which shows that for $R_\rho = 1$, the effective turbulence would be 3 orders of magnitude larger than the molecular value. The formulas derived by Kelley (1984) and Fedorov (1988) give for $R_\rho = 1$ a $k_{TE} \sim 10^{-4}$, which is of the same order. However, the corresponding salt diffusity is

$$k_{SE} = \tau^{1/2} k_T = 0.1 k_{TE}, \tag{41}$$

in contrast to the $k_{TE} \sim k_{SE}$ for $R_\rho = 1$ obtained by Kelley. This difference is not surprising considering the different flux laws employed.

We may note that k_{TE} depends upon the value used for the critical Rayleigh number. A larger Ra_* leads to larger effective diffusivity. This may at first appear surprising. However, a higher Ra_* requires larger and more buoyant parcels, which can rise further and form deeper layers. The smaller the number of interfaces present, the more effective becomes the vertical transfer.

5.2. *Summary*

The present approach has involved many assumptions but it contains few adjustable parameters. The only free choices are the depth of the unstable layer and the critical Rayleigh number and these cannot be taken completely at random.

The value used for Ra_* holds for a linear profile and two free boundaries. In the present case the profile is not linear and only one boundary exists. Spangenberg and Rowland (1961) observed that a Rayleigh number of 1200 was needed to trigger the convection from a free evaporating surface. Once the convection had started, the Rayleigh number between the plumes was about 100. The adopted value should be reasonable and since t_* and δ_{i*} do not depend strongly on Ra_*, a moderately different choice would not lead to significant changes.

The representation of δ_{i*} is more serious. If the depth of the entire unstable layer is used, the results will be altered. The time needed for the instability to become critical is shorter and the turbulence production less intense, while the fluxes and the migration of the interface are larger. The lowering of the critical time increases with increasing property steps. It will be about 10–20% and probably negligible for case (b). However, for case (c) the critical time might be reduced by a factor of 2. Since $w_* \sim t_*^{-1/2}$ this means, that the migration of the interface would increase by 40%.

The turbulence production depends strongly on the velocity of the plumes and to use Stokes' resistance law, valid for a sphere, to obtain the terminal velocity of a plume is at least questionable. This also goes for the estimate of the diameter of the parcel. Since the velocity varies as the square of the diameter, this introduces significant uncertainties. Moreover, to apply Stokes' law, the Reynolds number should be less than 1. Tables 1 and 4 show that the Reynolds number is about 5 and some contribution to the turbulence is likely to be overlooked.

The two-dimensional description of the convection process simplifies the calculations. However, it has support in laboratory experiments. Spangenberg and Rowland (1961) concluded that two-dimensional motions dominated the convection and at the boundary. Observed axi-symmetric plumes were transient and evolved into plunging sheets or line plumes. The assumed dynamics would not be able to sustain an axi-symmetric plume, since by mass continuity, it would require a larger acceleration towards the plume than can be accomplished by the evolving pressure gradient.

6. Acknowledgment

I wish to thank Ulf Jonasson at the Oceanography Department in Göteborg for doing the numerical computations and Hans Friedrich at the Institut für Merreskunde in Hamburg for his comments. This work grew out of studies carried out together with Arne Foldvik at the Geophysical Institute in Bergen, while I held a scholarship from the Nordic University Group on Physical Oceanography, and which was continued at the Norwegian Polar Research Institute. Financial support was partly granted by the Deutsche Forschungsgemeinschaft (SFB 318).

7. Appendix: List of symbols

Numerical constants and abbreviations used in the equations are not given.

H	Depth of the homogeneous layer.
H_0	Maximum rise of the buoyant plumes.
k_{SE}	Effective eddy diffusivity for salt.
k_{TE}	Effective eddy diffusivity for heat.
L_*	Horizontal spacing between the plumes.
M	Kinetic energy of the horizontal motion at the interface.
Q	Buoyancy flux.
R_ρ	$=\rho_S\rho_T^{-1}$, ratio of the density contributions.
Ra	Rayleigh number.
Ri	Richardson number.
S	Salinity.
T	Temperature.
U	Horizontal velocity at the interface.
W	Vertical velocity of the plumes.
W_0	Terminal vertical velocity.
e	Entrainment velocity.
f	Concentration of any property.
g	$=9.8\ \mathrm{m\ s^{-2}}$. Acceleration of gravity.
i	$=1, 2$ subscript indicating the different layers.
p'	Perturbation pressure.
t	Time.
u_*	r.m.s. velocity.
w_*	Migration velocity of the interface.
x	Horizontal coordinate.
z	Vertical coordinate.
z_m	Level of maximum density anomaly.
z_0	Level of zero density anomaly.
ϕ	Flux of any property.
δ_i	Thickness of the layer of unstable density gradient.
$\delta_{\rho i}$	Diameter of buoyant parcels.
δ_T	Penetration depth of heat.
ε	Turbulent energy production.
k_S	$=10^{-9}\ \mathrm{m^2\ s^{-1}}$ diffusion coefficient of salt.
k_T	$=10^{-7}\ \mathrm{m^2\ s^{-1}}$ diffusion coefficient of heat.
ν	$=1.5\cdot10^{-6}\ \mathrm{m^2\ s^1}$ coefficient of viscosity.
ρ	$=1000\ \mathrm{kg\ m^{-3}}$ average density.
ρ_{0i}	Initial density.
ρ_S	Density contribution due to salt.
ρ_T	Density contribution due to heat.
ρ'	Density anomaly.
$\Delta\rho_i$	Density anomaly in the unstable parcel.
τ	$=k_S k_T^{-1}$ ratio of the diffusion coefficients.
$*$	Subscript indicating critical value.

REFERENCES

Batchelor, G. K. 1967. *An introduction to fluid dynamics.* Cambridge Univ. Press, 615 pp.

Carmack, E. C. 1986. Circulation and mixing in ice-covered waters. In: *The geophysics of sea-ice.* (ed. N. Untersteiner), New York, Plenum Press, 641–712.

Chandrasekhar, S. 1961. *Hydrodynamic and hydromagnetic stability.* Oxford, Clarendon Press.

Fedorov, K. N. 1988. Layer thickness and effective diffusivities in "diffusive" thermohaline convection in the ocean. In: *Small-scale turbulence and mixing in the ocean.* (eds. J. C. J. Nihoul and B. M. Jamart), Amsterdam, Elsevier, 471–479.

Fernando, H. J. S. 1989. Oceanographic implications of laboratory experiments on diffusive interfaces. *J. Phys. Oceanogr. 19*, 1707–1715.

Foldvik, A. and Rudels, B. 1979. *Double-diffusive convection into deep homogenous layers.* Geophysical Institute, Div. A. Univ. of Bergen, Norway. Report 53, 22 pp.

Foster, T. D. and Carmack, E. C. 1976. Temperature and salinity structure in the Weddell Sea. *J. Phys. Oceanogr. 6*, 36–44.

Howard, L. N. 1967. Convection at high Rayleigh number. In: *Proc. 11th Int. Congr.* Applied Mechanics, München (ed. H. Görtler). Berlin, Springer-Verlag, 1109–1115.

Huppert, H. E. 1971. On the stability of a series of double-diffusive layers. *Deep-Sea Res. 18*, 1005–1021.

Kelley, D. E. 1984. Effective diffusivities within ocean thermohaline staircases. *J. Geophys. Res. 89*, 10484–10488.

Kelley, D. E. 1988. Explaining effective diffusivities within diffusive oceanic staircases. In: *Small-scale mixing and turbulence in the ocean.* (eds. J. C. J. Nihoul and B. M. Jamart), Amsterdam, Elsevier, 481–502.

Kelley, D. E. 1990. Fluxes through diffusive staircases: a new formulation. *J. Geophys. Res. 95*, 3365–3371.

Linden, P. F. and Shirtcliffe, T. G. L. 1978. The diffusive interface in double-diffusive convection. *J. of Fluid Mechanics 87*, 417–432.

Mamayev, O. I. 1975. *Temperature-salinity analysis of the world ocean waters.* Amsterdam, Elsevier, 374 pp.

McDougall, T. J. 1981a. Double-diffusive convection with a non-linear equation of state. Part I: The accurate conservation of properties in a two-layer system. *Progr. in Oceanogr. 10*, 71–89.

McDougall, T. J. 1981b. Double-diffusive convection with a non-linear equation of state. Part II: The relative importance of cabbeling and double-diffusive convection. *Progress in Oceanography 10*, 91–121.

Schmitt, R. W., Lueck, R. G. and Joyce, T. M. 1986. Fine and microstructure at the edge of a warm-core ring. *Deep-Sea Res. 33*, 1665–1689.

Shirtcliffe, T. G. L. 1973. Transport and profile measurements of the diffusive interface in double-diffusive convection with similar diffusivities. *J. Fluid Mech. 57*, 27–43.

Spangenberg, W. G. and Rowland, W. R. 1961. Convective circulation in water induced by evaporative cooling. *Phys. of Fluids 4*, 743–750.

Turner, J. S. 1965. The coupled turbulent transports of salt and heat across a sharp density interface. *Int. J. Heat and Mass Trans. 8*, 759–767.

Turner, J. S. 1973. *Buoyancy effects in fluids.* Cambridge, Cambridge Univ. Press, 367 pp.